Macromolecular Materials and Engineering
Open Access
www.mame-journal.de

Antimicrobial Brushes on Titanium via "Grafting to" Using Phosphonic Acid/Pyridinium Containing Block Copolymers

Rafael Methling, Oliver Dückmann, Frank Simon, Cornelia Wolf-Brandstetter, and Dirk Kuckling**

Coating medical implants with antibacterial polymers may prevent postoperative infections which are a common issue for conventional titanium implants and can even lead to implant failure. Easily applicable diblock copolymers are presented that form polymer brushes via "grafting to" mechanism on titanium and equip the modified material with antibacterial properties. The polymers carry quaternized pyridinium units to combat bacteria and phosphonic acid groups which allow the linear chains to be anchored to metal surfaces in a convenient coating process. The polymers are synthesized via reversible-addition-fragmentation-chain-transfer (RAFT) polymerization and postmodifications and are characterized using NMR spectroscopy and SEC. Low grafting densities are a major drawback of the "grafting to" approach compared to "grafting from". Thus, the number of phosphonic acid groups in the anchor block are varied to investigate and optimize the surface binding. Modified titanium surfaces are examined regarding their composition, wetting behavior, streaming potential, and coating stability. Evaluation of the antimicrobial properties revealed reduced bacterial adhesion and biofilm formation for certain polymers, albeit the cell biocompatibility against human gingival fibroblasts is also impaired. The presented findings show the potential of easy-to-apply polymer coatings and aid in designing next-generation implant surface modifications.

1. Introduction

Dental implants are a commonly used treatment with increasing demand due to the longer lifespans of the population and a rising interest in cosmetic dentistry.[1] Still, complications or even implant failure are regularly observed and may require intensive aftercare or revision surgery.[2] One of the main reasons is the accumulation of bacterial biofilms, which in >50% of all implantations lead to peri-implant mucositis, an inflammation of the soft tissue surrounding the implants. If this inflammation is left untreated the disease can progress to peri-implantitis affecting also the alveolar bone.[3]

Successful implantation relies on osseointegration. Thus, implants are usually made of titanium or titanium alloys which show good biocompatibility, however, they are also prone to bacterial infections due to low intrinsic antibacterial properties.[4] Many strategies for altering the surface to overcome these drawbacks have been published, both physical[5] or chemical in nature.[6,7,8] Hydrophobic cationic polymers have been identified as a class of antibacterial agents and are extensively investigated, for example as a substitute for conventional antibiotics or as means to render surfaces contact-killing,[9,10] especially considering that bacteria seem less likely to build up resistance against them.[11]

The widely accepted mechanism for antibacterial polymers in solution is based on the close contact of the positively charged polymer and the negatively charged cell membrane due to electrostatic attraction. Subsequently, hydrophobic moieties insert into the membrane, leading to its disruption and cell death.[12] However, as immobilized polymers lack degrees of freedom compared to molecules in solution, the mechanism of action is not yet understood. Hence, the mobility of the chain and final orientation of cationic and hydrophobic patches might be crucial in a similar way as shown for antimicrobial peptides.[13]

The immobilization of polymer chains is mainly possible by either a "grafting from"-approach, i.e., a low-molecular compound is bound to the surface and the polymerization is started there, or by "grafting to", meaning that ready-made polymer chains bind to the surface from solution.[14] The latter allows for an

R. Methling, O. Dückmann, D. Kuckling
Department of Chemistry
Paderborn University
Warburger Straße 100, 33098 Paderborn, Germany
E-mail: dirk.kuckling@uni-paderborn.de
F. Simon
Leibniz-Institut für Polymerforschung Dresden
Hohe Straße 6, 01069 Dresden, Germany
C. Wolf-Brandstetter
Max Bergmann Center of Biomaterials
Technische Universität Dresden
Budapester Str. 27, 01069 Dresden, Germany
E-mail: cornelia.wolf-brandstetter@tu-dresden.de

The ORCID identification number(s) for the author(s) of this article can be found under https://doi.org/10.1002/mame.202200665

DOI: 10.1002/mame.202200665

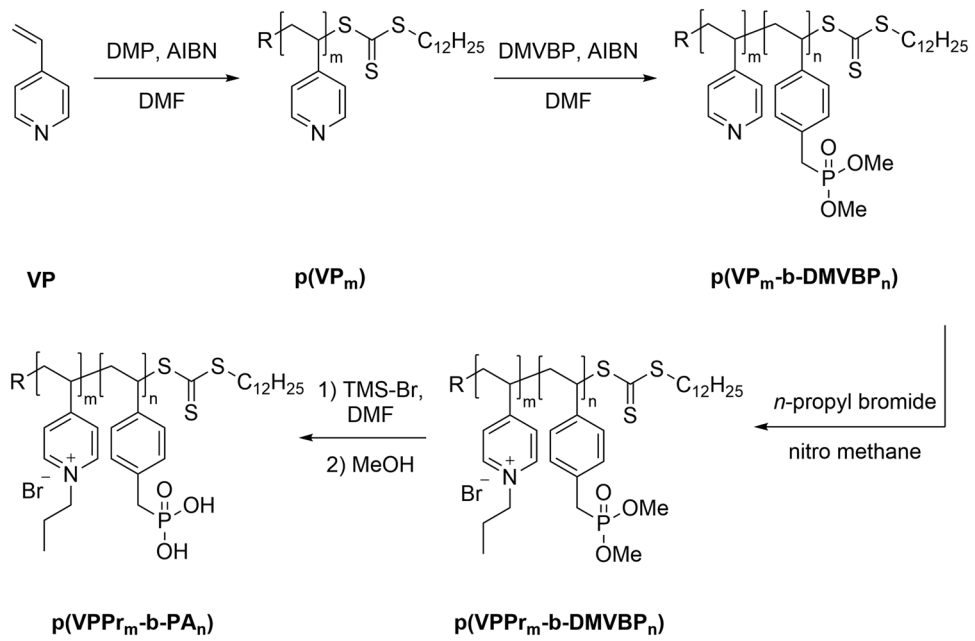

Scheme 1. The general method for synthesizing diblock copolymers p(VPPr$_m$-b-PA$_n$).

easy preparation and analysis of a well-defined polymer with the drawback of generally lower grafting densities compared to "grafting from".[15]

In polymer brushes, chains are connected to the surface via one terminal moiety which is able to form one (e.g., thiols,[16] silanes[17]) or more (e.g., catechols,[18] phosphonic acids[19]) covalent bonds with the surface, sometimes aided by hydrogen bonding. There have also been systems investigated that make use of longer segments containing anchoring groups, however, there is little information on why a specific quantity is chosen.[20,10] To the best of our knowledge, the effect of the quantity of phosphonic acid groups in linear polymer blocks on the grafting density has not been investigated yet.

Hence, a set of antibacterial diblock copolymers comprising anchoring blocks in varying lengths and a second segment with alkylated pyridinium moieties at a fixed length is presented. The anchor block is equipped with phosphonic acid moieties to allow for the formation of polymer brushes on titanium oxide surfaces via "grafting to". Phosphonic acids have frequently been employed for grafting organic molecules to metals via condensation reaction with surface hydroxyl groups and show better hydrolytic stability than siloxanes, for example.[21] Quaternized poly(4-vinyl pyridinium) was chosen as second block due to its established antibacterial efficacy which can easily be modified by exchanging the alkyl halides used for post modification.[7,22] The grafting density on titanium oxide particles depending on the anchor block length is examined and the surface properties of the polymer brushes are investigated concerning the zeta potential and stability in low and high pH environments. Antibacterial effects were evaluated using cell adhesion assays and the cell biocompatibility towards human gingival fibroblasts was assessed.

Table 1. Molecular masses (NMR and SEC), dispersities *D*, and solubility in methanol and water for diblock copolymers.

Polymer	M_n (NMR) [g mol^{-1}]	M_n (SEC) [g mol^{-1}]	*D*	Sol. in MeOH/H_2O
p(VPPr$_{65}$-b-PA$_3$)	16000	15500	1.38	✓/✓
p(VPPr$_{65}$-b-PA$_6$)	16400	15400	1.52	✓/✓
p(VPPr$_{65}$-b-PA$_{16}$)	18300	17200	1.60	✓/✓
p(VPPr$_{65}$-b-PA$_{21}$)	19700	15900	1.44	✓/*X*
p(VPPr$_{65}$-b-PA$_{48}$)	24600	insoluble	–	*X*/*X*
p(VPPr$_{65}$-b-PA$_{114}$)	37000	insoluble	–	*X*/*X*
p(PA$_{11}$-b-VPPr$_{66}$)[a]	17500	18700	1.89	✓/✓

[a] reverse block order

2. Results and Discussion

2.1. Synthesis

A series of block copolymers were prepared by RAFT polymerization of **VP** and isolation of the macro-RAFT agent, followed by polymerization of a second block using **DMVBP** as a monomer (**Scheme 1**).

The length of **p(VP)** was fixed to 65 and 66 units based on published research on comparable systems with good antibacterial effectiveness in that range.[10] The ratio of **DMVBP** was varied to obtain different anchor block lengths (**Table 1**). In order to investigate possible effects of block sequence, polymer **p(PA$_{11}$-b-VPPr$_{66}$)** was synthesized in reversed order. The conversion was determined via ^{1}H-NMR of the quenched reaction mixture by comparison of monomer and polymer signals. After

purification, pyridine groups were alkylated with 1-bromopropane to yield cationic hydrophobic moieties which exhibit strong bactericidal effects while still being well-soluble in polar solvents. Analyses via NMR spectroscopy reveal a quantitative quaternization. Last, phosphonic acids are produced in a two-step reaction utilizing TMSBr and methanol which is verified by the characteristic shift of the corresponding resonance from 29 ppm to 26 ppm via ^{31}P NMR spectroscopy (Figures S2 and S3, Supporting Information). The peak of the phosphonic acid is more pronounced upon the acidification of the sample with hydrochloric acid.

The formation of homo and diblock copolymers is revealed by SEC measurements showing monomodal distributions through every synthetic step and the derived masses are in good agreement with the values calculated from NMR results (Figure S4, Supporting Information). With dispersities ranging from 1.38 to 1.60, the molecular mass distribution of the final polymers is slightly broader than to be expected under optimized RAFT-conditions except for **p(PA$_{11}$-b-VPPr$_{66}$)** where the reverse order negatively impacts *D* with a value of 1.89. Still, we anticipate no negative impact on the desired function of the adsorbed brush. The overall solubility in polar solvents decreases with increasing number of phosphonic acid groups in the anchor block resulting in **p(VPPr$_{65}$-b-PA$_{21}$)** not being soluble in water and **p(VPPr$_{65}$-b-PA$_{48}$)** and **p(VPPr$_{65}$-b-PA$_{114}$)** not being soluble in water or alcohols at all.

2.2. Adsorption on Titanium Oxide Particles

As titanium samples carry a native oxide layer, we used titanium oxide particles to investigate the affinity of polymer to the metal surface from methanolic solutions at different concentrations.[23] Phosphonic acid groups react with surface hydroxyl groups to form M-O-P bonds, covalently anchoring the polymer to the particle. Visually, the adsorption becomes evident as the coated particles behave like a stable dispersion for several hours up to days, whereas the pristine titanium oxide particles settle without stirring in a shorter timeframe.

Generally, higher polymer concentrations lead to higher grafting densities (**Figure 1**). Samples with 3, 6, 11, and 16 **PA**-units plateau at ≈2.5 to 3.0 mmol L^{-1} (≈50 mg mL^{-1}). This agrees with the notion that there are no multilayers formed but the saturation of the surface is reached at a certain threshold. **p(PA$_{11}$-b-VPPr$_{66}$)** was synthesized in a reverse block order which does not have a significant effect on the adsorption efficacy. Grafting densities up to 0.75 µmol m^{-2} are reached which is in the same order of magnitude as reported values for polymer brushes formed by the "grafting to"-mechanism.[15,17,24,25] A comparison of different block lengths shows that the adsorption efficacy is dependent on the anchor block length with **p(VPPr$_{65}$-b-PA$_{21}$)** performing best. This, however, goes at the cost of solubility in water (and other solvents at even higher content of **PA**) which should be considered when designing polymers for coating titania as this may be a critical factor in the treatment process of implant surfaces.

Noticeably, the polymers with higher molecular masses yield the highest grafting density which contradicts the common observation that the grafting density is partly controlled by the polymer mass, i.e., shorter polymer chains allow for a denser

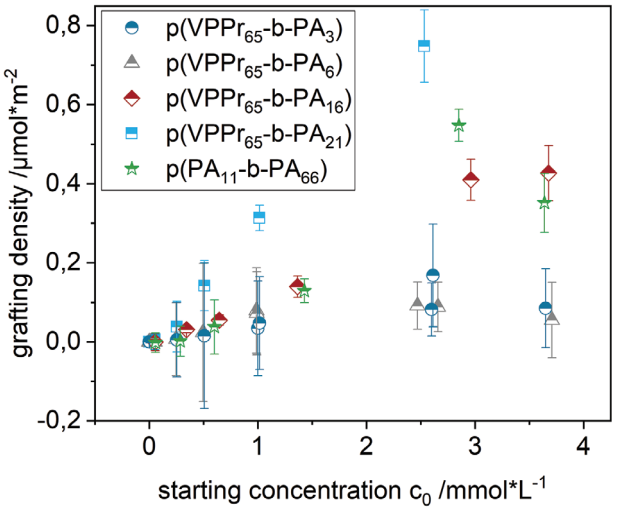

Figure 1. Grafting density of adsorbable diblock copolymers on titanium oxide particles at different concentrations.

occupation.[26] It is suggested that the diffusion of new chains to the surface is facilitated when the neighboring polymer strands occupy less space, resulting in more chains per area. However, recent findings indicate that the grafting and degrafting are not only limited by diffusion but also by intricate processes at the reactive site with the involvement of the binding groups.[24] Since the polymers reported here contain more than one binding site, the effect of polymer mass may well be overcompensated by this.

Of the various polymers synthesized, three water-soluble compounds were selected for further surface modification and biological characterization, which, due to their molecular composition, allow the influence of two different aspects to be investigated. Comparing **p(VPPr$_{65}$-b-PA$_3$)** and **p(VPPr$_{65}$-b-PA$_{16}$)**, conclusions can be drawn regarding higher or lower grafting densities. Since **p(VPPr$_{65}$-b-PA$_{16}$)** and **p(PA$_{11}$-b-VPPr$_{66}$)** form polymer brushes of similar density, they allow insights into the effect of reverse block order.

2.3. Physicochemical Properties of Coated Titanium Samples

For the titanium reference, an intermediate hydrophilicity was observed with of ≈45° in static contact angle measurements with water (**Figure 2**). All polymer-coated surfaces exhibited even lower contact angles, but the difference to the reference was significant only for **p(VPPr$_{65}$-b-PA$_3$)**. For this coating type, the shorter length of the hydrophobic anchor block could modify the wettability of the coated surfaces the most. However, the differences between the three selected polymer coatings were only partially significant, i.e., between the polymer coatings with the shortest and longest anchor blocks, respectively. In addition to static measurements, dynamic contact angle measurements were also performed (Figure S8, Supporting Information), in which local inhomogeneity is better compensated for. Here, similar trends were seen, with higher variability on coated samples compared to uncoated references, slightly indicating a heterogeneous coating result.

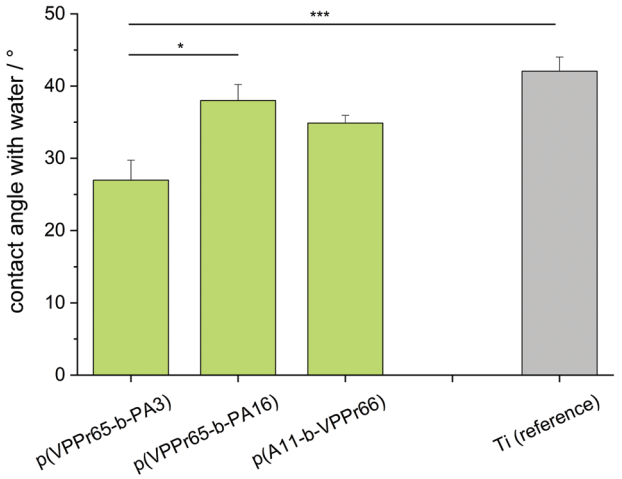

Figure 2. Static contact angles determined with water.

Coated and identically treated reference samples were analyzed by means of X-ray photoelectron spectroscopy (XPS) after identical treatment steps as for all further physicochemical and biological characterizations. A typical wide scan as well as high-resolution spectra of C and N region of the reference and one polymer coated sample are shown in **Figure 3**. The atomic percentages of the components most relevant for the interpretation of coating results are shown in **Table 2**, while complete analysis is given in (Tables S3 and S4, Supporting Information).

The high-resolution element spectra were deconvoluted into component peaks having different binding energy values (BE). The shapes of N 1s spectra recorded from the copolymer-coated samples are very characteristic for the **p(VPPr$_m$–b–PA$_n$)** polymer. The two well-separated component peaks indicate the presence of two differently bonded nitrogen species. On first look, these findings are in contrast to the suggested chemical structure of the synthesized polymers showing only one species of nitrogen as well as NMR data revealing complete quaternization. Photoelectrons from these protonated nitrogen species (C–^{M}N^{+} = C ↔ C = ^{M}N^{+}–C) led to component peak *M* at BE ≈ 402.39 eV. The binding energy values of the second component peak *L* (BE ≈ 399.93 eV) is characteristic for organically bonded nitrogen atoms that do not carry a charge, such as C–^{L}N = C ↔ C = ^{L}N–C. However, the amount of charge of a quaternary nitrogen can also be compensated by strong electrostatic interactions with an electron donor, e.g. titanates (Ti–O$_y$) from the titanium oxide surface. Similar peak splittings of quaternary ammonium compounds partially interacting with surfaces have been found on silanoates (Si–O$_y$).[27]

Care should be taken when interpreting the calculated atomic percentages, as it is well known that the native titanium oxide layer can be contaminated with a number of hydrocarbon impurities from the laboratory atmosphere or from the solutions used for the cleaning and coating steps. Typically, a variety of different compounds containing alcohols, ethers, ketones, and carboxyl groups are found. During the coating process, the polymers are expected to adsorb in addition to already existing contaminations or to partially replace them. The resultant C content thus is based on remaining contaminations as well as on the presence of adsorbed polymers. In contrast, the N and P can be regarded as marker elements for the success of polymer adsorption. As shown in Table 2, a clear increase of the P content was observed for the three polymers having the same block order and differing only in the anchor block length (**p(VPPr$_{65}$-b-PA$_3$)**, **p(VPPr$_{65}$-b-PA$_{16}$)**, **p(VPPr$_{65}$-b-PA$_{21}$)**). With increasing P content in the polymers also increasing P was found on coated samples. As the pyridinium block was of constant length, the increasing N content indicates a higher polymer coating density for the polymers with longer phosphonate anchor block in accordance with the adsorption experiments shown in Figure 1. The behavior of the polymer **p(PA$_{11}$-b-VPPr$_{66}$)** with reversed block order was obviously different. While the P content fits to the relative percentage of P within the molecule, less N was found in adsorbed state. However, this sample was also found to have higher Ti and O content and lower C content, making this coating in parts more similar to the uncoated reference sample than the other coated samples. Hence a different orientation of adsorbed molecules might be expected. Different behavior of this compound is also seen when comparing molecular weight specified by size exclusion chromatography, revealing the highest hydrodynamic radius although NMR studies revealed a molecular weight according to the sum formula.

Titanium reference samples as well as polymer-coated samples were further characterized by streaming potential measurements. The calculated ζ potential shows a nearly linear slope in the region close to the IEP which suggests chemically inert surfaces for all types of samples (Figure 3). For the polymer-coated samples this is in agreement with the expected behavior of the polycationic blocks, i.e., the part that extends into the surrounding solution, as alkylated pyridinium as well as the polymer backbone is generally unreactive. For the reference surface IEPs between pH 3.3 and 3.8 were determined in repeated measurements. This value is slightly lower compared to previous measurements of titanium surface by streaming potential measurement in our own group[28] and by others[29] reporting an IEP of ≈4.0. This difference in surface properties of our reference surfaces can be attributed to the pretreatment by autoclaving within ultrapure water, resulting in a much more hydrophilic surface with contact angles of only 45°. The autoclaving of titanium is known to increase the native oxide layer,[30] which then dominates at the surface, while titanium surfaces stored at air tend to adsorb hydrocarbon contaminations. In consequence, a higher content of dissociable acidic OH-groups is expected comparable to the observed increase, when titanium surfaces were heated in water vapor.[31] The behavior of the polymer-coated surface is obviously dominated by the positively charged VPPr-block, as all three coatings with the identical VPPr block result in very similar ζ potential curves with identical IEP and slope. The IEP is significantly shifted by roughly 3 pH units towards higher pH compared to the uncoated reference with values ranging between pH 6.5 and 7. The surface charge properties were neither affected by the different lengths of the anchor groups nor by the order of the two blocks (**p(VPPr$_{65}$-b-PA$_{16}$)** versus **p(PA$_{11}$-b-VPPr$_{66}$)**) **Figure 4**.

2.4. Brush Stability Measurements

The formation of a polymer brush on titanium surfaces as well as its stability towards acidic and basic conditions were investigated

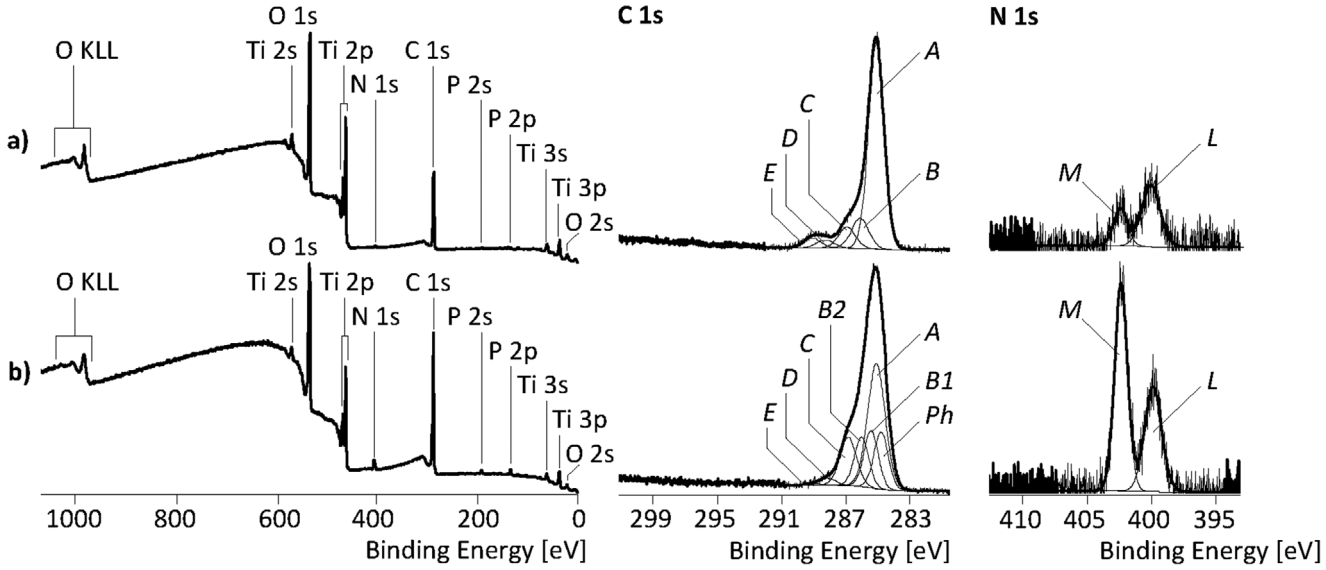

Figure 3. XPS wide-scan (left column), C 1s (middle column), and N 1s (right column) spectra for a) uncoated titanium reference and b) polymer-coated sample **p(VPPr$_{65}$-b-PA$_{16}$)**. The assignment of the component peaks (*Ph*, *A*, *B*, etc.) to the structural units can be found in the Figure S9, Supporting Information.

Table 2. Relative elemental compositions of reference and polymer-coated samples as derived from XPS survey spectra. More data on elemental composition derived for other elements be found in supporting information Tables S3 and S4.

Peak	C 1s [At%]	N 1s [At%]	O 1s [At%]	P 2p [At%]	Ti 2p3/2 [At%]
Reference (Ti)	48.25	1.01	37.26	0.38	11.94
p(VPPr$_{65}$-b-PA$_3$)	58.84	2.35	29.05	1.03	7.35
p(VPPr$_{65}$-b-PA$_{16}$)	59.73	2.97	27.56	1.49	6.70
p(VPPr$_{65}$-b-PA$_{21}$)	64.78	2.93	23.79	2.02	5.45
p(PA$_{11}$-b-VPPr$_{66}$)	55.12	2.56	31.05	1.31	8.41

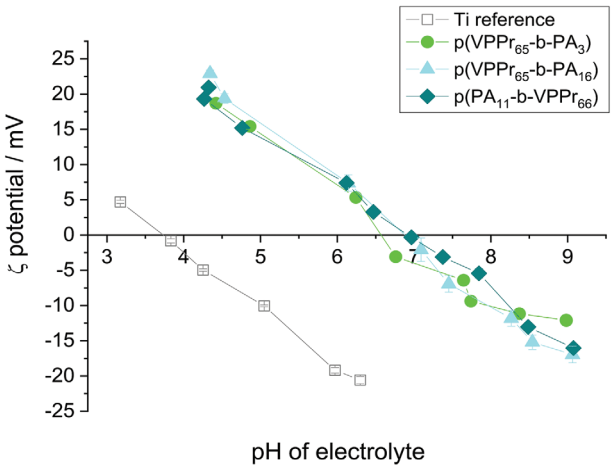

Figure 4. Streaming potential measurements at different pH values allowing the calculation of ζ potential of coated samples.

via surface plasmon resonance (SPR) spectroscopy. This method allows the in situ investigation of thin layers on metal coated wafers regarding their thickness and refractive indices. Conducting time-dependent measurements, kinetic phenomena like adsorption and desorption can be monitored.[23,32] The substrate is LaSFN9-glass coated with chromium (≈1 nm), gold (≈50 nm), and titanium oxide (≈4 nm). **p(VPPr$_{65}$-b-PA$_{16}$)** was chosen as a representative sample due to its high grafting density and water solubility to prepare the polymer brush on the metal layer via "grafting to".

The significant shift in the plasmon-minimum from 57.1° to 60.2° (**Figure 5A**) after the coating process proves the formation of an additional layer. The thickness of the polymer adlayer is derived from fitting the angle-dependent reflectivity to the edge of total internal reflection and the plasmon minimum assuming a refractive index of the swollen polymer layer of 1.435 (ϵ' = 2.06, detailed parameters in Tables S1 and S2, Supporting Information). Thus, a layer thickness of 9 nm was determined which is in the expected range for grafted polymer brushes in good solvents.[24]

The brush stability was probed in aqueous media using a flow cell by observing changes in reflectivity over time (Figure 5B). After equilibration, a stable baseline is afforded which suggests that there is no desorption in water. Dental implants are exposed to considerable chemical stress due to food intake, which is why acidic and basic conditions were used to probe the sample. Exposure to aqueous hydrobromic acid (pH 2) over 10 min does not affect the layer thickness significantly. Injection of aqueous sodium hydroxide (pH 12), however, causes a considerable drop in reflectivity, corresponding to a shift of the plasmon minimum to lower angles. Fitting the resulting curves reveals a decrease in thickness from 9 nm to ≈5 nm. Remarkably, the chains are only partly removed from the surface. It has been established that polyelectrolyte brushes are inherently more strained than their noncharged counterparts: due to intramolecular repulsion of

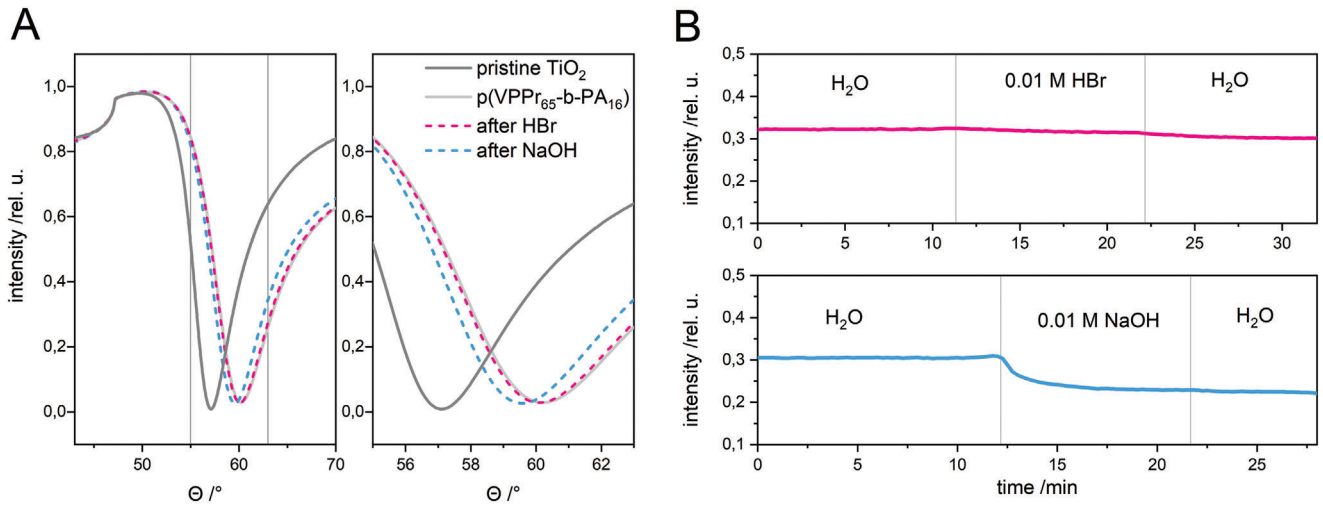

Figure 5. SPR measurements: A) full reflectivity scans of titanium oxide surface coated with **p(VPPr$_{65}$-b-PA$_{16}$)** before and after exposure to HBr/NaOH and B) stability test against water and 0.01 M HBr/NaOH in kinetic mode.

adjacent cationic groups the polyelectrolyte assumes a more stretched conformation which results in a loss of entropy and decreases the energy necessary for mechanical failure of the surface-polymer-bonds.[17] Particularly, high grafting densities decrease the thermodynamic stability of polyelectrolyte brushes due to intermolecular repulsion of neighboring strands. The results suggest that after a certain number of chains have been cleaved, the hydrolytic stability is improved owing to a more relaxed conformation of the remaining molecules ("mushroom" regime[33]).

2.5. Microbiological and Cell Biological Investigations of Coated Titanium Samples

Data on amounts of detached viable bacteria shown in **Figure 6** represent the extent of bacteria able to survive at the surface after 17 h of biofilm formation. Respective bacteria were detached by combined sonification and vortexing for subsequent quantification. In contrast, the live/dead staining images (**Figure 7**) reflect conditions directly on the samples immediately after biofilm formation.

Bacterial adhesion and subsequent biofilm formation at the titanium surfaces was significantly reduced ($p < 0.001$) at samples coated with **p(VPPr$_{65}$-b-PA$_3$)** or **p(PA$_{11}$-b-VPPr$_{66}$)**, while antibacterial effect was limited for coatings with **p(VPPr$_{65}$-b-PA$_{16}$)**. Here, the viability of detachable bacteria was even slightly higher than on uncoated reference surfaces (Figure 6), although obviously a higher number of dead cells was also found in contact with this surface compared to the reference (Figure 7). In general, a higher percentage of dead cells was observed for all coated polymers compared to the uncoated reference, but complete killing was not achieved.

The difference in the antibacterial properties of **p(VPPr$_{65}$-b-PA$_3$)** and **p(VPPr$_{65}$-b-PA$_{16}$)**, was surprising, as both differ solely in the length of the anchor block, but not in quaternized pyridinium block. These findings are in line with the outcomes of the cytotoxicity assays described further below. However, when

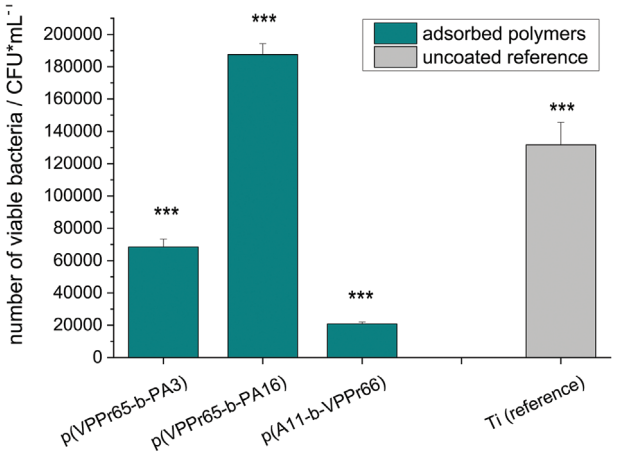

Figure 6. Characterization of coated titanium samples with respect to their antibacterial potential: Number of viable bacteria attached to the surfaces after 17 h cultivation under starving conditions promoting biofilm formation (Asterisks denote significant differences to all other sample types).

redissolved polymers were in contact with planktonic bacteria (Figure S6, Supporting Information) similar antimicrobial efficacy was observed for both polymers differing in anchor block length but with identical quaternized block.

A very interesting finding is the significantly different behavior of bacteria to polymers with a comparable length of both blocks but a reversed block order, **p(PA$_{11}$-b-VPPr$_{66}$)** versus **p(VPPr$_{65}$-b-PA$_{16}$)**, which was observed in adsorbed state as well as for dissolved polymers (Figure 6 and Figure S6, Supporting Information). Interpretation of the XPS spectra indicate a different orientation as P content was comparable but the higher Ti and O content could be explained by a thinner coating. Due to the reversed synthesis of blocks, the polymer brushes carry different end groups facing the solution. As a result of the macro-RAFT agent, **P(PA$_{11}$-b-VPPr$_{66}$)** features a terminal aliphatic dodecyl chain, whereas the polycationic block of **p(VPPr$_{65}$-b-PA$_{16}$)**

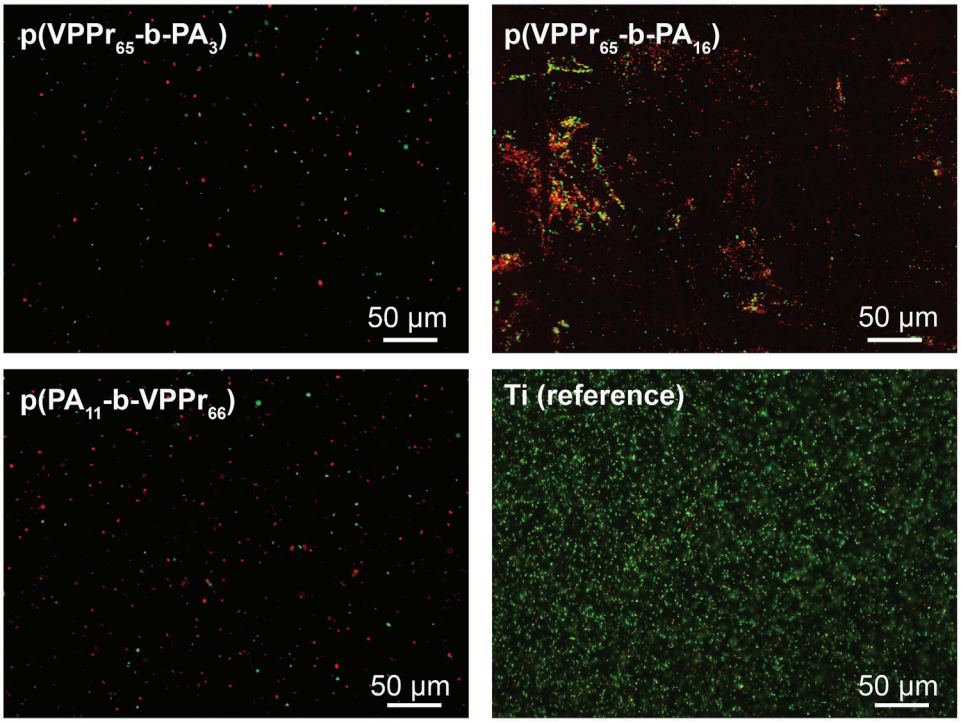

Figure 7. Live/dead staining of attached biofilm directly after dynamic cultivation.

is terminated with a carboxylic acid group. The difference in hydrophilicity may affect the orientation on the surface and thus the interaction with biological systems and are subject of ongoing research.

In addition to the polymer-based effects, it has to be highlighted that the biofilm adhesion at reference surfaces, that were polished and stored under wet conditions prior to all experiments, was already comparatively low with an ≈2-log reduction compared to machined and grinded surfaces used in previous investigations for identical cultivation conditions.[34] By additional functionalization with the polymers, the adhesion of viable bacteria could be further reduced in particular by **p(PA$_{11}$-b-VPPr$_{66}$)**.

Cell biocompatibility was assessed with polymer-coated samples (**Figure 8**) as well as with polymer solutions directly diluted in cell culture medium (Figure S8, Supporting Information). Cell adhesion and cell spreading were impaired in a manner that goes in line with the antibacterial properties: only slight changes in cellular behavior was seen for **p(VPPr$_{65}$-b-PA$_{16}$)**, while reduced cell attachment and as well as less expressed cell spreading are seen for coatings with **p(VPPr$_{65}$-b-PA$_3$)** or **p(PA$_{11}$-b-VPPr$_{66}$)**. This correlation between antimicrobial activity and cytotoxicity is known for a series of other antimicrobial substances such as polymers based on (2-methacryloyloxyethyl) phosphonate (DMMEP) and dipicolyl aminoethyl methacrylate (DCAMA) copolymers.[8]

3. Conclusion

Seven linear block copolymers containing polycationic pyridinium segments and phosphonic acid anchor blocks were synthesized via RAFT polymerization and postmodifications. Using a "grafting to" process to form polymer brushes on titanium substrates, it was observed that the grafting density increased with the number of phosphonic acid groups present in the anchoring block. The brushes proved stable in neutral and acidic conditions, while basic conditions diminished the grafting density to a certain degree.

The antimicrobial activity of the polymers could be verified for all three selected water-soluble molecules but was depended on actual design and immobilization status. When exclusively the anchor block length was changed an equal antimicrobial effect was seen for dissolved polymers in contact with planktonic bacteria.

In contrast, for adsorbed polymers antimicrobial efficacy was greater for the shorter anchor block, although a higher surface density was achieved for the longer anchor block length. Final explanations for this behavior are not possible with actual available data, but might be related to the higher flexibility of the cationic **VPPr**-block of the molecule with a shorter anchor block in the adsorbed state. Another interesting impact factor was identified, as the reversed blockchain order of phosphonic anchor and cationic **VPPr**-block had a tremendous effect on antimicrobial efficacy but cytotoxic properties as well, although an identical shift of the IEP was obtained, and thus overall surface chemistry should be comparable. Of particular high interest is to find out the reasons for this completely different biological behavior. Potential effects might be attributed to the specific conformation of polymers in an immobilized state, as the molecular weight order was reversed in NMR and size exclusion experiment, indicating a higher hydrodynamic radius of the polymer with the reversed block order. Different binding status was also derived from XPS measurements. For this aspect further investigations to specify surface orientation are required to discrim-

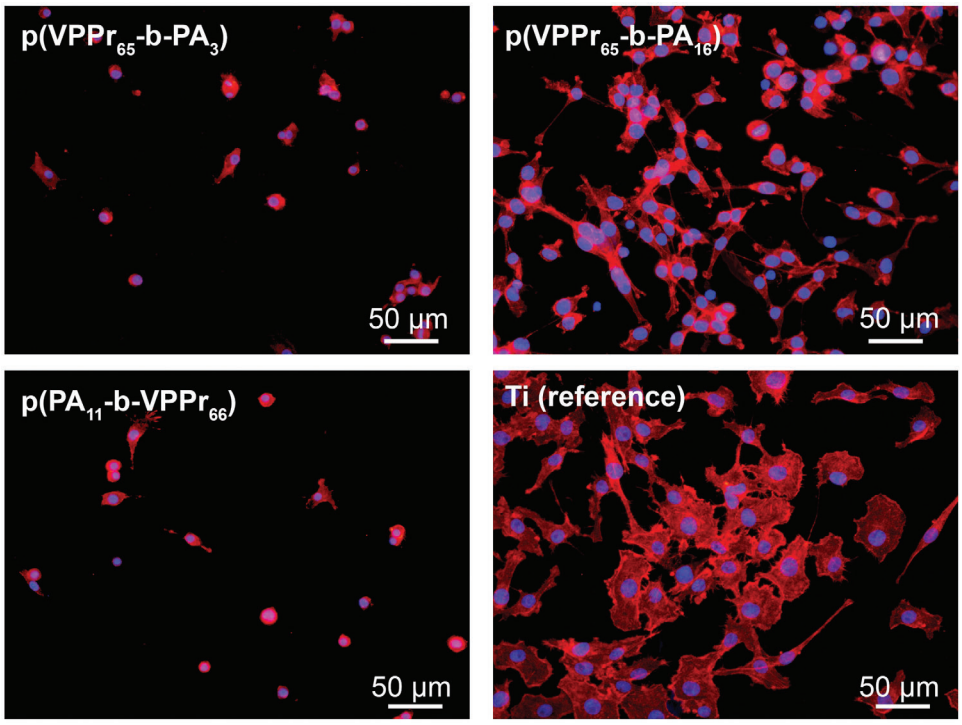

Figure 8. Assessment of the biocompatibility of coated titanium samples: Fluorescence images of human gingival fibroblast after 24 h cell adhesion to coated titanium samples with staining for nuclei (blue) and actin (red).

inate physicochemically-based effects from additional impact factors.

4. Experimental Section

Materials: 4-vinylbenzyl chloride (90%) and 4-vinyl pyridine (**VP**, 95%) were purchased from Merck and distilled before use. AIBN (98%) was purchased from Merck and recrystallized from ethanol before use. Titanium oxide particles (Aeroxide P25), 2-(Dodecylthiocarbonothioylthio)-2-methylpropionic acid (DMP, 98%), trimethyl phosphite and trimethylsilyl bromide (TMSBr, 97%) and LB medium were purchased from Merck and used as received. Dulbecco's Modified Eagle Medium (DMEM), 10% fetal bovine serum, glutamate, penicillin, and streptomycin were purchased from Merck Biochrom. Human gingival fibroblasts (HGF) were purchased from CellBiologics, Chicago, IL. 1-bromopropane and nitromethane were purchased from Acros Organics. DMF (extra dry over molecular sieves) was purchased from Thermo Scientific. Methanol (HPLC grade) was purchased from Carl Roth. Acetone, diethyl ether, ethyl acetate, *n*-hexane, and toluene were technical grade solvents.

Synthesis: *Dimethyl 4-Vinylbenzyl Phosphonate* (***DMVBP***): 4-vinylbenzyl chloride (15 mL, 90.8 mmol) was reacted with trimethyl phosphite (45 mL, 345.0 mmol) with traces of BHT as a radical scavenger at 110 °C under argon atmosphere for 19.5 h. Excess phosphite was removed in vacuo and the raw product was isolated via column chromatography (*n*-hexane/ethyl acetate 1:1, then ethyl acetate/acetone 1:1), which yielded **DMVBP** as a colorless oil (6.19 g, 27.4 mmol, 30%).

^{1}H-NMR (DMSO-*d6*, 700 MHz) δ (ppm): 3.26 (d, $^{2}J_{PH}$ = 21.7 Hz, 2H, P–C**H**$_2$), 3.60 (d, $^{3}J_{PH}$ = 10.8 Hz, 6H, O–C**H**$_3$), 5.24 (dt, $^{2}J_{HH}$ = 1.0 Hz, $^{3}J_{HH}$ = 10.9 Hz, 1H, CH–C**H**$_{trans}$), 5.80 (dt, $^{2}J_{HH}$ = 1.0 Hz, $^{3}J_{HH}$ = 17.6 Hz, 1H, CH–C**H**$_{cis}$), 6.71 (dd, $^{3}J_{HH}$ = 10.9 Hz, $^{3}J_{HH}$ = 17.7 Hz, 1H, Ar–C**H**$_2$), 7.24-7.43 (m, 4H, Ar–**H**); ^{13}C-NMR (DMSO-*d6*, 176 MHz) δ (ppm): 31.4 (Ph–**C**H$_2$), 52.8 (O–**C**H$_3$), 114.4(CH–**C**H$_2$), 126.6 (Ar–**C**), 130.4 (Ar–**C**), 132.5 (CH$_2$–**C**), 136.2 (CH–**C**), 136.8 (CH$_2$–**C**H); ^{31}P-NMR (DMSO-*d6*, 202 MHz) δ (ppm): 28.95 (s, 1P); HRMS (ESI) *m/z*: [M + Na$^+$] calcd for $C_{11}H_{15}O_3PNa$: 249.0657 g mol^{-1}, found: 249.0651 g mol^{-1}.

RAFT Polymerization: In a typical reaction, **VP** (3064.0 mg, 29.14 mmol), DMP (129.6 mg, 0.36 mmol), and AIBN (8.8 mg, 0.05 mmol) were dissolved in dry DMF (10 mL) in a Schlenk tube with a rubber septum and a stirring bar. The solution was purged with argon for 30 min and placed in a preheated oil bath at 70 °C afterward. After stirring for 17 h, the reaction was quenched by freezing the mixture with liquid nitrogen and exposure to air. For the determination of monomer conversion, a sample was taken and examined by ^{1}H NMR spectroscopy. The polymer was precipitated from toluene (250 mL), collected by filtration, and dried in vacuo, yielding p(4VP$_{65}$) (2037.1 mg, 64%, 85% monomer conversion) as red solid.

^{1}H-NMR (DMSO-*d6*, 500 MHz) δ (ppm): 0.81–0.85 (br, 3H, $C_{11}H_{22}$—C**H**$_3$), 1.17–1.25 (br, 20H, C_{10}**H**$_{20}$), 1.25–2.26 (br, 204H, C**H**$_2$–C**H**), 6.39–6.99 (br, 136H, Ar–**H**), 7.99–8.51 (br, 136H, Ar–**H**)

In a typical block copolymer synthesis, **p(VP$_{65}$)** (277.8 mg, 0.04 mmol) was employed as macro-RAFT agent, and placed a Schlenk tube with a rubber septum and a stirring bar. After the addition of **DMVBP** (221.0 mg, 0.98 mmol) and AIBN (1,2 mg, 0.01 mmol), the compounds were dissolved in dry DMF (5 mL) and the solution was purged with argon for 30 min. The reaction vessel was placed in a preheated oil bath at 70 °C for 20 h and quenched afterward by freezing the mixture with liquid nitrogen and exposure to air. For the determination of monomer conversion, a sample was taken and examined by ^{1}H NMR spectroscopy. The polymer was precipitated from cold diethyl ether (125 mL, −95 °C), collected by filtration, and dried in vacuo, which afforded **p(VP$_{65}$-b-DMVBP$_6$)** (304.0 mg, 61%, 34% monomer conversion) as beige solid.

^{1}H-NMR (DMSO-*d6*, 500 MHz) δ (ppm): 0.82–0.86 (br, 3H, $C_{11}H_{22}$–C**H**$_3$), 1.17–1.26 (br, 20H, C_{10}**H**$_{20}$), 1.27–2.27 (br, 222H, C**H**$_2$–C**H**), 3.08-3.25 (br, 12H, P–C**H**$_2$), 3.46–3.63 (br, 36H, O–C**H**$_3$), 6.23–7.21 (br, 160H, Ar–**H**), 7.99–8.48 (br, 136H, Ar–**H**); ^{31}P-NMR (DMSO-*d6*, 202 MHz) δ(ppm): 29.0–29.4 (br, 1P)

Post Modifications—Amine Quaternization: In a typical reaction, **p(VP$_{65}$-b-DMVBP$_6$)** (282.5 mg, 0.03 mmol) were reacted with

1-bromopropane (590 µL, 0.64 mol) in nitromethane (6 mL) at 60 °C for 24 h. Due to precipitation from the reaction mixture, nitromethane (4 mL) was added and the slightly turbid solution was stirred at 70 °C for 6 h. The polymer was precipitated from diethyl ether (200 mL), collected by filtration, and dried in vacuo, which afforded **p(VPPr$_{65}$-b-DMVBP$_6$)** (483.3 mg, 88%) as green solid.

^{1}H-NMR (DMSO-*d6*, 500 MHz) δ (ppm): 0.69–1.08 (br, 207H, NCH_2CH_2–C**H**3 and $C_{11}H_{22}$–C**H**$_3$), 1.16–1.26 (br, 20H, C_{10}**H**$_{20}$), 1.30–2.44 (br, 358H, NCH_2–C**H**$_2$ and C**H**$_2$–C**H**), 3.18–3.26 (br, 12H, P–C**H**$_2$), 3.44–3.65 (br, 36H, O–C**H**$_3$), 4.15–5.00 (br, 136H, N–C**H**$_2$), 6.26–7.21 (br, 24H, P-CH_2-Ar–**H**), 7.69–9.42 (br, 272H, Pyr-**H**); ^{31}P-NMR (DMSO-*d6*, 202 MHz) δ(ppm): 28.6-29.7 (br, 1P)

Phosphonate Ester Methanolysis: In a typical reaction, **p(VPPr$_{65}$-b-DMVBP$_6$)** (463,3 mg, 0.03 mmol) was dissolved in dry DMF (11 mL) under argon atmosphere. The solution was cooled with an ice bath and TMS-Br (0.3 mL, 2.3 mmol) were added with a syringe. The mixture was stirred overnight at 40°C and volatiles were removed *in vacuo* afterward. Methanol (15 mL) was added to the residue and stirred for 2 d. After dialysis and lyophilization of the reaction mixture, **p(VPPr$_{65}$-b-PA$_6$)** (296.9 mg, 64%) was afforded as a brown solid.

^{1}H-NMR (DMSO-*d6*, 500 MHz) δ (ppm): 0.66-1.11 (br, 207H, NCH_2CH_2-C**H**3, and $C_{11}H_{22}$-C**H**$_3$), 1.19-1.28 (br, 20H, C_{10}**H**$_{20}$), 1.32-3.14 (br, 358H, NCH_2-C**H**$_2$, and C**H**$_2$-C**H**), 3.18-3.26 (br, 12H, P-C**H**$_2$), 4.35-4.88 (br, 136H, N-C**H**$_2$), 6.42-7.24 (br, 24H, P-CH_2-Ar-**H**), 7.57-9.43 (br, 272H, Pyr-**H**); ^{31}P-NMR (DMSO-*d6*, 202 MHz) δ(ppm): 21.4-23.8 (br, 1P); Traces of conc. *HCl* were added to the NMR sample of ***p(VPPr$_{65}$-b-PA$_6$)*** to make PA resonances visible.

Titanium References and Polymer-Coated Samples: Flat discs of commercially pure titanium grade 2 with sample sizes of 10 mm diameter and 2 mm height were obtained with a mirror polish surface finish from Viktor Hegedüs GmbH (Germany). These samples were cleaned by subsequent ultrasonic baths of 2% Triton x-100, acetone, ethanol, and ultrapure water. In the next step, the samples were autoclaved lying in ultrapure water and stored under these sterile and wet conditions. Immediately prior to start of each experiment, the samples were dried in a laminar flow bench. Coating of samples was performed with 2 mM of each polymer dissolved in methanol (p.a.) covering the complete surface for 2 h in a small closed container saturated with methanol vapor. Subsequently, the samples were washed under vigorous shaking with 1 mL of phosphate-buffered saline (PBS), followed by two rinsing steps with 1 mL of ultrapure water, each for 5 min. The samples were then air-dried in a laminar flow bench and directly used for subsequent analyses. Reference samples were treated identically with adsorption step performed with pure methanol.

Analysis: For information on instrumentation, see SI.

Adsorption Isotherms: For each polymer, UV/vis-spectra of solutions in methanol (0.01 mg mol^{-1} – 0.2 mg mol^{-1}) were recorded for calibration (Figure S5, Supporting Information). Adsorption experiments were conducted by adding the respective amount of polymer and Aeroxide P25 (5 mg) to methanol (1 mL). After treating the samples for 10 min in an ultrasonic bath, they were stirred for 2–4 h. The dispersions were filtered through syringe filters. The resulting solutions were diluted with methanol until the absorption was in the calibrated range and their UV/vis-spectra were recorded to determine the concentration of residual polymer.

SPR Sample Preparation and Measurement: Surface plasmon resonance (SPR) measurements were performed using a He-Ne laser with a wavelength of 623.8 nm in Kretschmann configuration. LaSFN9 glass wafers were coated via ALD with chromium (ca. 1 nm), gold (≈50 nm), and titanium oxide (≈4 nm), respectively. For the grafting process, the wafer was overlayed with a solution of **p(VPPr$_{65}$-b-PA$_{16}$)** (33 mg) in methanol (1 mL) overnight. Afterward, the remaining liquid was removed with a pipette and the sample was dried in a compressed nitrogen flow. It was annealed in an oven at 120 °C for 24 h and thoroughly washed with methanol and absolute ethanol. For kinetic measurements, the angle was set to the flank left to the plasmon minimum at ≈30% reflectivity.

Contact Angle Measurements: Static and dynamic contact angle measurements were conducted with an OCA-30 (DataPhysics, Germany) using ultrapure water with samples stored at air no longer than 1 d. The images of the drops lying on top of the surface (8 µl) of advancing and receding drops were recorded with the internal camera and subsequently analyzed with the software provided by the manufacturer. The initial drop size was also 8 µl and pictures and dosing speed during measurements was set to 0.1 µL s^{-1}. Receding angles could not be determined for all surfaces but were rather comparable with values close to or below 10°.

Streaming Potential Measurements: Measurements of ζ potential were performed by means of a commercial electrokinetic analyzer (EKA, Anton Paar GmbH, Austria) equipped with a gap cell. For each experiments a set of two discs was mounted via double-sided tape onto sample holders resulting in a parallel orientation and the channel was adjusted to 150 µm. The electrolyte consisted of 0.001 M KOH, that was automatically titrated with 0.1 M HCl and 0.1 M KOH in a pH range of 3.0 – 9.0. Pressure profiles were recorded in two directions from 0 to 250 mbar and four measurement points per titration step were analyzed. The ζ potential values were calculated from determined streaming potential according to the Fairbrother-Mastin method by means of software supplied by the manufacturer.

Analysis of Attachment and Biofilm Formation Under Starving Conditions: The bacteria adhesion experiment was conducted as described in Kaiser et al. in more detail.[34] In brief, coated titanium samples and respective uncoated reference samples, all disinfected with UV irradiation for 30 min, were seeded by placing 100 µL of a bacteria suspension of *E. coli* SM2997 containing 10^8 colony forming units (CFU)/mL onto the surfaces for 1 h at 30 °C. After this, the bacteria suspension was removed and immediately rinsed 3 times with 100 µL phosphate-buffered saline (PBS). Cultivation of samples with remaining attached bacteria was continued under dynamic conditions for 17 h at 30 °C hanging in reverse position in 24 well plates filled with 1.2 mL biofilm (BF) medium per well (see the receipt for this medium in Kaiser et al.[34]). The fraction of bacteria being only weakly attached was removed by three washing steps with 1.2 mL PBS under shaking for 5 min. Subsequently, the attached bacteria were completely removed by three consecutive steps of vortexing, ultrasonic bath, and repeated vortexing (30 s each) with the samples placed in 50 ml Falcon tubes filled with 1 mL of LB medium. The number of viable bacteria was determined by means of a proliferation assay described in detail elsewhere.[34]

Live/dead Staining: Staining of the samples was performed with the LIVE/DEAD kit (Invitrogen) according to the manufacturer's instructions after 17 h of biofilm formation as described above, followed by the three rinsing steps with PBS. Staining of individual samples was conducted immediately prior to fluorescence microscopy. Pictures were taken with a cLSM 510 meta (Zeiss, Jena, Germany).

Biocompatibility Assessment: Titanium samples coated with antimicrobial polymers as described above were disinfected by 30 min UV irradiation. Afterward they were transferred to 48 well plates (Nunclon Delta, Nunc) and cell seeding was performed by the addition of 1 mL cell suspension containing 5.000 primary human gingival fibroblasts. Cells were used in 7th passage and cultivated in Dulbecco's Modified Eagle Medium (DMEM) supplemented with 10% fetal bovine serum, 2 mM glutamate, 100 U penicillin, and 100 µg ml^{-1} streptomycin.

After 24 h of cultivation, the samples were washed with PBS and fixed with 3.7% formaldehyde solution for 20 min at 4 °C. Prior to staining cells were permeabilized with 0.2% Triton X-100 in PBS for 2 min and then incubated for 1 h with 2 µg mL^{-1} of 4′,6-Diamidino-2-phenyl-indol-dihydrochlorid, 2-(4-Amidinophenyl)-6-indolcarbamidin-dihydrochlorid (DAPI) and AlexaFluor 546 Phalloidin (Invitrogen), diluted 1:40 in PBS. Samples were analyzed with a cLSM 510 meta (Zeiss, Germany) equipped with a CCD camera.

Statistical Analysis: Bacterial experiments were carried out in duplicate, with each individual experiment performed with $n = 4$. All results are shown as mean ± standard error. Statistical analysis was performed using one-way Anova, with Levene's test for equal variances and Tukey's post hoc test with respective correction for multiple comparisons of means. Significant differences were assumed at $p < 0.05$. Significant differences are assigned in the graphs by use of asterisks with * for $p < 0.05$, ** for $p < 0.01$, and *** for $p < 0.001$.

X-ray photoelectron spectroscopy (XPS): All XPS studies were carried out by means of an Axis Ultra photoelectron spectrometer (Kratos Analytical, Manchester, UK). The spectrometer was equipped with a monochromatic Al Kα ($h \cdot \nu = 1486.6$ eV) X-ray source of 300 W at 15 kV. The kinetic

energy of photoelectrons was determined with a hemispheric analyzer set to pass energy of $E_{pass} = 160$ eV for wide-scan spectra and $E_{pass} = 20$ eV for high-resolution spectra. During all measurements, electrostatic charging of the sample was avoided by means of a low-energy electron source working in combination with a magnetic immersion lens. Later, all recorded peaks were shifted by the same value that was necessary to set the C 1s peak to 285.00 eV. Quantitative elemental compositions were determined from peak areas using experimentally determined sensitivity factors and the spectrometer transmission function. Spectrum background was subtracted according to Shirley.[35] The high-resolution spectra were deconvoluted by means of the Kratos spectra deconvolution software. Free parameters of component peaks were their binding energy (BE), height, full width at half maximum, and the Gaussian-Lorentzian ratio.

Supporting Information

Supporting Information is available from the Wiley Online Library or from the author.

Acknowledgements

Open access funding enabled and organized by Projekt DEAL.

Conflict of Interest

The authors declare no conflict of interest.

Data Availability Statement

The data that support the findings of this study are available from the corresponding author upon reasonable request.

Keywords

antimicrobial polymers, antimicrobial surfaces, grafting to, polymer brushes

Received: January 31, 2023
Published online: February 19, 2023

[1] F. Accioni, J. Vázquez, M. Merinero, B. Begines, A. Alcudia, *Pharmaceutics* **2022**, *14*, 455.
[2] B. Al-Nawas, P. W. Kämmerer, T. Morbach, C. Ladwein, J. Wegener, W. Wagner, *Clin. Implant Dent. Relat. Res.* **2012**, *14*, 127.
[3] a) H. Dreyer, J. Grischke, C. Tiede, J. Eberhard, A. Schweitzer, S. E. Toikkanen, S. Glöckner, G. Krause, M. Stiesch, *J. Periodontal. Res.* **2018**, *53*, 657; b) L. J. A. Heitz-Mayfield, G. E. Salvi, A. Mombelli, P.-J. Loup, F. Heitz, E. Kruger, N. P. Lang, *Clin. Oral. Implants Res.* **2018**, *29*, 1.
[4] a) F. Rupp, L. Liang, J. Geis-Gerstorfer, L. Scheideler, F. Hüttig, *Dent. Mater.* **2018**, *34*, 40; b) Y. Wang, Y. Zhang, R. J. Miron, *Clin. Implant Dent. Relat. Res.* **2016**, *18*, 618.
[5] S. Bierbaum, S. Mulansky, E. Bognár, I. Kientzl, P. Nagy, N. E. Vrana, M. Weszl, E. Boschke, D. Scharnweber, C. Wolf-Brandstetter, *Biomater. Sci.* **2018**, *6*, 1390.
[6] a) V. Sambhy, B. R. Peterson, A. Sen, *Angew. Chem., Int. Ed. Engl.* **2008**, *47*, 1250; b) W. Heuer, A. Winkel, P. Kohorst, A. Lutzke, C. Pfaffenroth, H. Menzel, F.r.-W. Bach, J. Volk, G. Leyhausen, M. Stiesch, *Adv. Eng. Mater.* **2010**, *12*, B609.
[7] J. C. Tiller, C.-J. Liao, K. Lewis, A. M. Klibanov, *Proc. Natl. Acad. Sci. USA 98*, **2001**, 5981.
[8] M. Waßmann, A. Winkel, K. Haak, W. Dempwolf, M. Stiesch, H. Menzel, *J Biomater Sci Polym Ed* **2016**, *27*, 1507.
[9] a) L. Sun, L. Song, X. Zhang, S. Yuan, S. Luan, *J. Mater. Sci. Technol.* **2022**, *126*, 191; b) L. Ringenberg, A. Winkel, O. Kufelt, P. Behrens, M. Stiesch, W. Heuer, *Int. J. Dent.* **2011**, *2011*, 859140; c) C. Pfaffenroth, A. Winkel, W. Dempwolf, L. J. Gamble, D. G. Castner, M. Stiesch, H. Menzel, *Macromol. Biosci.* **2011**, *11*, 1515.
[10] L. Liu, W. Peng, X. Zhang, J. Peng, P. Liu, J. Shen, *J. Mater. Sci. Technol.* **2021**, *62*, 96.
[11] H.-S. Joo, C.-I. Fu, M. Otto, *Philos. Trans. R. Soc. London, Ser. B* **2016**, 371.
[12] Y. Yang, Z. Cai, Z. Huang, X. Tang, X.i Zhang, *Polym J* **2018**, *50*, 33.
[13] a) K. A. Brogden, *Nat. Rev. Microbiol.* **2005**, *3*, 238; b) J. M. Ageitos, A. Sánchez-Pérez, P. Calo-Mata, T. G. Villa, *Biochem. Pharmacol.* **2017**, *133*, 117.
[14] G. Ye, J. Lee, F. Perreault, M. Elimelech, *ACS Appl. Mater. Interfaces* **2015**, *7*, 23069.
[15] S. Rauch, K.-J. Eichhorn, D. Kuckling, M. Stamm, P. Uhlmann, *Adv. Funct. Mater.* **2013**, *23*, 5675.
[16] F. Zhou, Z. Zheng, B.o Yu, W. Liu, W. T. S. Huck, *J. Am. Chem. Soc.* **2006**, *128*, 16253.
[17] M. Menzel, W.-L. Chen, K. Simancas, H. Xu, O. Prucker, C. K. Ober, J. Rühe, *J. Polym. Sci., Part A: Polym. Chem.* **2019**, *57*, 1283.
[18] B. Liang, E. Jia, X. Yuan, G. Zhang, Z. Su, *Chem. Eng. J.* **2020**, *401*, 126114.
[19] K. Babu, R. Dhamodharan, *Nanoscale Res. Lett.* **2008**, *3*, 9093.
[20] X. Zhang, L.i Liu, W. Peng, X. Dong, Y. Gu, Z. Ma, D. Gan, P. Liu, *J. Mater. Chem. B* **2021**, *9*, 4169.
[21] a) G. Guerrero, J. G. Alauzun, M. Granier, D. Laurencin, P. H. Mutin, in *Dalton Transactions*, Royal Society of Chemistry, Cambridge, England **2013**, Vol. *42*, p. 12569; b) P. H. Mutin, G. Guerrero, A. Vioux, *J. Mater. Chem.* **2005**, *15*, 3761; c) S. Marcinko, A. Y. Fadeev, *Langmuir* **2004**, *20*, 2270; d) B. M. Silverman, K. A. Wieghaus, J. Schwartz, *Langmuir* **2005**, *21*, 225.
[22] M. Topuzogullari, *J. Polym. Res.* **2018**, *25*, 2101.
[23] D. Kuckling, K. Moosmann, J. E. S. Schier, A. Britze, *Colloid Polym. Sci.* **2013**, *291*, 1429.
[24] M. Laus, R. Chiarcos, V. Gianotti, D. Antonioli, K. Sparnacci, G. Munaò, G. Milano, A. De Nicola, M. Perego, *Macromol. Chem. (Oxford)* **2021**, *54*, 499.
[25] a) D. Antonioli, R. Chiarcos, V. Gianotti, M. Terragno, M. Laus, G. Munaò, G. Milano, A. De Nicola, M. Perego, *Polym. Chem.* **2021**, *12*, 6538; b) M. K. Corbierre, N. S. Cameron, R. B. Lennox, *Langmuir* **2004**, *20*, 2867.
[26] L. Michalek, K. Mundsinger, C. Barner-Kowollik, L. Barner, *Polym. Chem.* **2019**, *10*, 54.
[27] B. P. Tripathi, P. Das, F. Simon, M. Stamm, *Eur. Polym. J.* **2018**, *99*, 80.
[28] S. Roessler, R. Zimmermann, D. Scharnweber, C. Werner, H. Worch, *Colloids Surf., B* **2002**, *26*, 387.
[29] K. Cai, M. Frant, J. Bossert, G. Hildebrand, K. Liefeith, K. D. Jandt, *Colloids Surf., B* **2006**, *50*, 1.
[30] B.oż Łosiewicz, P. Osak, J. Maszybrocka, J. Kubisztal, S. Stach, *Materials* **2020**, *13*, 4154.
[31] B. Feng, J. Y. Chen, S. K. Qi, L. He, J. Z. Zhao, X. D. Zhang, *J. Mater. Sci.: Mater. Med.* **2002**, *13*, 457.
[32] N. Horn, M. Kreiter, *Plasmonics* **2010**, *5*, 331.
[33] W. J. Brittain, S. Minko, *J. Polym. Sci., Part A: Polym. Chem.* **2007**, *45*, 3505.
[34] F. Kaiser, D. Scharnweber, S. Bierbaum, C. Wolf-Brandstetter, *Bioelectrochemistry* **2020**, *133*, 107485.
[35] D. A. Shirley, *Phys. Rev. B* **1972**, *5*, 4709.

